(4)

AN INVESTIGATION OF THE RECHARGEABILITY OF CERTAIN MODIFIED FORMS OF MnO_2

Final Report to

The Office of Naval Research

Contract No. NOO14-87-C-0662

Principal Investigator: John O'M. Bockris

Contributors: A. John Appleby
Oliver J. Murphy
Hari P. Dhar

Ementeck, Inc.
Route 5, Box 946A
College Station
Texas 77840

September 1988

SUMMARY

The modified form of MnO_2 prepared through doping with bismuth or lead possesses rechargeable properties. The work performed under this project was to investigate these properties. The bismuth modified MnO_2 (designated as MnO_2^*) was prepared by coprecipitation of hydroxides from the aqueous solutions of nitrates of Mn and Bi and subsequent oxidation of the hydroxides to the MnO_2^*.

The potentiodynamic cycling of this material in an electrochemical half-cell showed well defined charge-discharge peaks and constant utilization over 500 cycles. The galvanostatic charge-discharge cycles are characterized by a flat discharge potential of -0.35 V (vs. Hg/HgO) that corresponds to a cell potential of approximately 1.1 V for the Zn-MnO_2^* combination. The galvanostatic cycling at a high current density of 653 mA/g of Mn showed that during 200 cycles, the utilization dropped from 75% to 20% of the theoretical two electron capacity at -0.4 V (vs. Hg/HgO) cut off. This rather unimpressive performance compared to the potentiodynamic study is attributed to an unoptimized cell, rapid charge-discharge rates and possible loosening of contact of the MnO_2^* material to the current collector.

Other features of the MnO_2^* material are as follows: The material could be heat treated to 475°C, still retaining its rechargeable characteristics. The density of the material increases as a function of heat treatment from a value of 4 g/cm^3 at 50°C to 4.7 g/cm^3 at 475°C.

Preliminary investigations of the Zn-MnO_2^* system in the presence of selected membranes were aimed at determining ways to prevent migration of the soluble zincate anion to the MnO_2^* electrode. Selected membranes and additives were tested. An improvement in the cyclability of the MnO_2^* electrode was achieved under certain circumstances. Extensive testings of the Zn-MnO_2^* systems are needed.

Investigations of the mechanism of rechargeability by the XRD technique was hampered by the lack of sufficient crystallinity of the MnO_2^* material. The interrupted voltammetry studies showed that the accumulation of species of approximate composition $MnO_{1.8}$ can be harmful to the rechargeability of the MnO_2^* species.

Li-MnO_2^* cells containing a nonaqueous electrolyte were fabricated. The cells showed good open circuit voltages in the range of 3.1 to 3.4 V, but good cycling behavior of these cells could not be obtained.

1. INTRODUCTION

The conventional alkaline Zn-MnO_2 batteries are rechargeable only with a shallow depth of discharge. The first step in the discharge may involve a reaction of the type

$$MnO_2 + H_2O + e \Rightarrow MnOOH + OH^-$$

and the fact that this reaction causes a dilation of the lattice is regarded by some researchers as one basic cause of the lack of repeated rechargeability, even in respect to this one electron discharge step. The second discharge step may cause a loss of conductance associated with the presence of hausmannite, Mn_3O_4.

The discovery by a Ford research team led by Wroblowa (1-3), that the addition to MnO_2 of varying amounts of Bi or Pb oxide makes it possible to attain rechargeability of the $Mn^{4+} \Rightarrow Mn^{2+}$ step involving two electrons, raised hopes of using MnO_2 in secondary Zn and Li batteries.

Ementeck, Inc. entered into an agreement with the Ford Motor company to develop rechargeable alkaline Zn-MnO_2 cells and nonaqueous-based Li-MnO_2 cells. This final report comprises the work done through a one man-year effort under U.S. Navy contract No. N00014-87-C-0662, on the rechargeable MnO_2 material.

The following topics were addressed:

1. Preparation and testing of rechargeability of the bismuth modified MnO_2 (designated in this report as MnO_2^*).
2. Potentiodynamic and galvanostatic experiments on MnO_2^* under various conditions.
3. Basic research on MnO_2^* material and Zn-MnO_2^* cells.
4. Mechanism of rechargeability of the MnO_2^* electrode.
5. Construction and preliminary testing of Li-MnO_2^* nonaqueous cells.

2. EXPERIMENTAL

2.1 Preparation of MnO_2^*

The modified form of manganese dioxide having a Bi content of 5 to 7.5 mole % of the amount of Mn was prepared by the method of coprecipitation from nitrates as outlined in U.S Patent 4,520,005 (1). A typical preparation procedure is as follows: 68.55g of $Mn(NO_3)\cdot 4H_2O$ was dissolved in 150 ml of water containing a drop of concentrated HNO_3. The solution was filtered to remove extreneous suspensions. 9.87g of $Bi(NO_3)_3\cdot 5H_2O$ was dissolved in a minimum amount (approximately 4ml) of concentrated HNO_3 at 70°C. The above two solutions were mixed and cooled to 1°C. 27g of NaOH was dissolved in 200ml of water and the solution cooled to 1°C. This solution was then added to the mixture of nitrates slowly with constant stirring. The resulting suspension was oxidized with oxygen for 24 hrs. The temperature was kept below 5°C. The slurry was then filtered and washed repeatedly with ultra-pure water. The filtered cake was washed in some preparations with 0.2M H_2SO_4 and then rinsed with water to pH 7. Subsequently, the product was heated at 50°C to constant weight.

In a slight variation of the above procedure, graphite powder was added in one preparation to the mixture of aqueous solutions of the needed chemicals prior to carrying out the coprecipitation. The resulting MnO_2^* produced a better utilization of Mn in the potentiodynamic scans. The obvious reason for the latter observation could be the achievement of a thorough mixing of the MnO_2^* with graphite during the coprecipitation.

2.2 Mixing of MnO_2^* with Graphite and Acetylene Black

The dried MnO_2^* was ground with a mortar and a pestle for approximately 15 min. and then mixed with graphite and sometimes also with acetylene black in various proportions in an electric blender for another 15 min. The mixing process sufficiently disperses the MnO_2^* with the conducting carbon and thus facilitates electrochemical measurements on the otherwise poorly conducting MnO_2^*.

2.3 Electrochemical Cells

Two types of electrochemical cells were used in the measurements. A half-cell assembly as shown in Fig. 1 was used initially to obtain potentiodynamic scans. The working electrode in the form of a paste, comprising typically of 100 mg of 1:70 mixture of

MnO_2^* and graphite, in 9M KOH and a gelling agent, carboxy methyl cellulose, was enclosed along with a small Pt or Ni gauze current collector in two layers of microporous polypropylene (Celgard 3401). This arrangement was found suitable for a relatively quick evaluation of a preparation. A Hg/HgO reference electrode was brought close to the working electrode through a Luggin capillary. A glassy carbon boat served as the counter electrode and the main vessel for the cell assembly.

Another electrochemical cell used was of a flat design comprising two removeable plexiglass parts. These parts had slots where electrodes could be placed and then assembled with nuts and bolts. A mixture of MnO_2^*, graphite and acetylene black with the gelling agent and the electrolyte was pressed into a pellet under a pressure of 10 ton psi on a nickel screen current collector. This electrode was placed against a Ni/NiOOH counter electrode in the plexiglass cell. Prior to use, the Ni/NiOOH counter electrode was charged-discharged a few times in 5M KOH against a larger Ni/NiOOH electrode at a current density of 5 mA/cm^2. During the final cycle, the Ni/NiOOH counter electrode was left in a state of charge corresponding to 33% of its initial capacity. Two layers of Celgard 3401 and one layer of Pellon 2581 (both being microporous polypropylene) separated the MnO_2^* working electrode from the Ni/NiOOH counter electrode in the flat cell. The potential of the MnO_2^* electrode in the flat cell was measured versus a Hg/HgO reference electrode in 9M KOH solution.

2.4 Electrochemical and Other Instrumentation

For potentiodynamic recording of cyclic voltammograms of MnO_2^* and galvanostatic recording of charge-discharge cycles of the MnO_2^* material, a PARC model 362 scanning potentiostat was used. A PARC model 173 potentiostat/galvanostat was also used in combination with a home-made electronic box for changing electrode polarity on recording charge-discharge cycles of the MnO_2^* material. Cyclic voltammograms were plotted on a HP model 7004B X-Y recorder and also a Yokogawa model 3025 X-Y recorder.

XRD data were obtained at the Department of Chemistry, Texas A&M University. SEM and TEM analyses were carried out at the Electron Microscopy Center, Texas A&M University.

3. RESULTS AND DISCUSSIONS

3.1 Tests for rechargeability of MnO_2^*

The rechargeability of all preparations of MnO_2^* were tested through observations of charge-discharge characteristic peaks during potentiodynamic scans of the MnO_2^* material in a half-cell. A typical potentiodynamic scan is shown in Fig. 2. The utilization of Mn as a percentage of theoretical two electron capacity was observed to be in the range of 80%-95% in most experiments. Figure 3 shows a potentiodynamic scan for electrolytic MnO_2 (International Common Sample No. 2.) Even though some rechargeability was observed, the utilization of Mn was near 10% in the first cycle.

Long term potentiodynamic cycling was carried out over 550 cycles. Such data are shown in Fig. 4. The utilization of Mn increased during the first few cycles (as normally the case for the modified MnO_2), remained steady for some time at 80%, then decreased to 57% during the first 250 cycles. On extending the charging potential to +0.45 V from the initial +0.1 V, the utilization increased to 65% and remained constant at this value for a further 300 cycles. The decrease of utilization from the initially high value of 80% was attributed partly to the splitting of the charging peak (Fig. 5) and excluding the capacity component associated with the more anodic peak during the charging process on using a low value of the upper potential limit. The characteristic profile of the discharge peak was not dependent on the range of the charging potential used. This is shown from the fact that the discharge peak shape remained independent of the charging potential range (Fig. 5).

3.2 Galvanostatic and Potentiodynamic Experiments on MnO_2^* Under Various Conditions

These experiments were carried out in the flat cell where pressed pellets could be used. It was observed during constant current experiments, as was also noted by the Ford research group, that the lost activity in the MnO_2^* electrode could be regained if the electrode was polarized during discharge half-cycles to approximately -1.0 V vs. Hg/HgO reference electrode. This is explained by the electrochemically initiated rejuvenation of the interaction of Bi species with the MnO_2 lattice. An experiment was thus carried out in which the working MnO_2^* electrode was polarized to -1.1 V in every cycle to see if constant activity could be maintained. Discharge curves for the MnO_2^* electrode at a constant current of 10 mA are shown in Fig. 6. The rate of discharge corresponded to 653

mA/g of Mn which is relatively high compared to a rate of 10-50 mA/g of Mn found in many practical situations. The discharge curves are characterized by a steady potential of -0.35 V vs. Hg/HgO that corresponds to a cell potential of approximately 1.1 V for the Zn-MnO_2* combination. The utilization of Mn achieved at various cut-off voltages is shown in Fig. 7. The utilization is seen to decrease to 20% of two electron capacity during 200 cycles. The reasons for this decrease have been thought to be the following: (a) an unoptimized cell; (b) rapid charging rate (653 mA/g of Mn) used, and (c) inadequate contact with the current collector.

To examine the importance of the contact of MnO_2* with the current collector and if an improvement in the contact was necessary, a porous nickel plaque was impregnated with the MnO_2* and tested in the flat cell. Figure 8 shows data from potentiodynamic scans. The utilization of Mn achieved was low--approximately 20%--but remained steady during the 75 cycle test conducted. Galvanostatic discharge curves for an impregnated Ni plaque electrode are shown in Fig. 9 at a high discharge current of 625 mA/g of Mn. The utilization of Mn achieved ranged from 15 to 55% depending on the polarization limit imposed during cycling. The data presented here for impregnated electrodes show encouraging features of stable performance, which maybe attributed to an improved contact of the MnO_2* to the current collector.

3.3 Basic Research on MnO_2* and Zn-MnO_2* Cells

The MnO_2* was heat-treated in the temperature range 50-475°C to determine the best temperature for dehydration of the material. The dehydration of MnO_2* is necessary prior to its use in a nonaqueous lithium battery. The heat treatment was carried out in a furnace in air at selected temperatures for two hours. A wight-loss/temperature plot is illustrated in Fig. 10. Approximately eighty percent of the water is lost at 175°C followed by a gradual water loss at higher temperatures. The temperature range of 250-400°C can be chosen for heat-treating MnO_2* prior to fabricating lithium nonaqueous batteries.

Since the density of MnO_2* is also of interest, a pyknometer was used in collecting such data for various heat-treated samples. Dry kerosine was used as the pyknometer solvent. The method was first tested with an electrolytic grade of MnO_2 (I.C. sample #2), whose density was found to be 4.3 g/cm^3, in good agreement with the reported value of 4.2 g/cm^3. The apparent density data for the heat-treated samples are illustrated in Fig. 11. The density increased from 4.1 to 4.6 g/cm^3 as the temperature of

the heat-treatment increased from 50 to 475 °C. Such a change in density is expected as the modified MnO_2 loses water with accompanying sintering of the material.

The discharge-charge characteriestics of the heat-treated materials were investigated in 9M KOH in a flat cell equipped with an innocuous counter electrode (Ni/NiOOH) and a Hg/HgO reference electrode. All the heat treated materials showed good rechargeability. The discharge-charge curves were obtained in the potential range of -0.6 to 0.2 V versus Hg/HgO at a sweep rate of 1 mV/s. This sweep rate corresponded to a very high discharge rate of approximately 4 Amp/g of Mn. The electrode was cycled until both the anode and cathode peak heights became constant. From the integrated charge associated with such peaks, the utilization of Mn was calculated as a percentage of the theoretical two electron capacity. The utilization versus temperature plot is illustrated in Fig. 12. The rapid discharge rates used explain the relatively low utilization obtained for these samples. On increasing the heat-treatment temperature, the utilization further decreases.

The surface areas for the heat-treated samples, obtained from mercury porosimetry data, are as follows: 50°C sample, 65m^2/g; 250°C sample, 56.6m^2/g; 475°C sample, 39.6 m^2/g.

The low utilization obtained for the heat-treated material at higher temperatures could be attributed partly to the decrease in surface area of the materials and to the consequent inadequate mixing of the materials with conductive additives.

Also, under this task, preliminary evaluation was made of the MnO_2* in combination with a zinc counter electrode and a few additives in the electrolyte. Two classes of membranes were evaluated: ZAMM series--radiation grafted acrylic acid based polypropylene membranes--obtained from RAI Corporation, Long Island, New York and a membrane from T&G Corporation of Lebanon, Connecticut. Additives added to the electrolyte were polyvinyl alcohol and sodium orthosilicate. All these tests were done while carrying out potentiodynamic scans in the bundle electrode configuration shown in Fig. 1 and also in the flat cell. Figure 13 shows the results for the ZAMM membranes of different thicknesses. Curve 1 for the 4 mil thick membrane is the best among the three curves shown. Figure 14 shows tests for the ZAMM membranes with additives in the electrolyte. The additions of poyvinyl alcohol and sodium silicate improve the performance of the cells. The action of additives in this case has been explained (5) in terms of the formation of polymeric zincate and charged micelles of colloidal zincate. In the case of

both additives, the migration of zincate through the membrane decreases and thus the cyclability of the MnO_2^* electrode increases.

The utilization of Mn also improves when the MnO_2^* electrode is polarized to the negative potential of -1.2 V (Hg/HgO) on discharge. In a practical system, a high negative polarization of the MnO_2^* electrode can be accommodated periodically during a discharge period through the installation of an electronic device in the charging unit. Figure 15 shows data for the T&G membrane and additional data for ZAMM membranes. The performance of the former membrane was initially good, but the membrane disintegrated in the KOH electrolyte during long exposure. The addition of D-sorbitol in the electrolyte gave rise to only a slight improvement.

The performance of a cell in the presence of a Zn counter electrode is less satisfactory because of the diffusion and migration of zincate ($Zn(OH)_4^{2-}$) anions to the MnO_2^* electrode . The zincate anion reacts with MnO_2^* to form hetaerollite, a compound which contributes to irreversibility of the MnO_2^* electrode.

$$2\ MnOOH + Zn(OH)_4^{2-} \Rightarrow Mn_2O_3 \cdot ZnO + 2OH^- + 2H_2O$$

3.4 Mechanism of Rechargeability of the MnO_2^*

Ford research workers were unable to unambiguously decide whether the rechargeability of manganese oxides, achieved by doping with trivalent bismuth and/or divalent lead, was due to structure-stabilizing factors or to the dopant-effected change of the redox pathway which avoids accumulation of non-rechargeable (or non-conducting, i.e., electrochemically non-active) intermediates. To resolve this fundamental issue, the following studies were undertaken:

3.4.1 XRD Study

The objective was to see whether Bi or Pb ion incorporate into sites different than other cations, which do not affect rechargeability of birnessites, and whose positions have previously been determined (4).

One of the main objections against the structure-stabilizing effect of these ions are the small amounts (down to approximately 1/100 Bi:Mn molar ratio) which are effective. However, if indeed bismuth and lead occupy *special* lattice sites (highly probable in view of the uniqueness of their ionic radii--no other cation is 1.2 Å in radius), they may exert,

even in small doping amounts, long-range forces which determine the lattice rearrangements necessary for reversibility of the redox processes. The long-range lattice effects of miniscule amounts of dopant are established in the literature for, e.g., the electrochemical response of graphite to traces of boron inserted into the layered structure (6).

In general, the products prepared by the coprecipitation method were less crystalline than those obtained by the exchange of Na in Na-birnessite with Bi or Pb. In most cases only two lines 7.2 and 3.6 Å regions were found in the XRD spectra. This was particularly true if the pressed disks were used for the XRD determination due to the preferred orientation of the layer structure. Minor peaks in the 2.4 and 2.3 Å regions were also observed in some samples. The positions of the broad lines at 7.0 and 3.5 Å showed that the basic $PbMn_xO_y$ and $BiMn_xO_y$ (washed with water only) were of the same structure as that of the Na-birnessite while that of the acid washed $BiMn_xO_y$ was similar to the acid washed Na-free birnessite, showing 7.2 and 3.6Å, $Mn_7O_{13} \cdot 5H_2O$. The latter could be converted to the former by contacting with KOH solution. The lack of adequate crystallinity of these materials prevented further indepth interpretation of the XRD data.

3.4.2 TEM and SEM Examination of MnO_2* Samples

The $NaMn_xO_y$ and $BiMn_xO_y$ prepared by coprecipitation and exchange methods were examined by the transmission electron microscope. These compounds all have very thin sheet structures. Elemental analyses of selected areas under the scanning electron microscope showed that the Mn/Bi intensity ratio of various areas of the sample varied within a narrow range. Thus, it ruled out the possibility that Bi and Mn exist as separate phases, at least for the samples with near stoichiometric Mn/Bi ratios.

3.4.3 Study of Cyclic Behavior of Lower Mn Oxides

The lack of rechargeability of conventional MnO_2 electrodes was variously ascribed to a number of factors (3). In order to pinpoint at which stage of the 2-electron redox process the non-rechargeable intermediate specie(s) appear, a systematic study was initiated of the cyclability of MnO, Mn_2O_3, and Mn_3O_4, both with and without Bi_2O_3 admixtures. Among important results obtained is that the non-rechargeable intermediate(s) appear around the Mn^{3+} stage of *reduction* and that doping with Bi^{3+} after this stage had been

reached *does not* impart rechargeability. However, *preoxidation of Mn_2O_3* and subsequent addition of Bi_2O_3 leads to rechargeable behavior of the electrode, as does admixing of Bi_2O_3 to MnO.

3.4.4 Interrupted Voltammetry of Modified MnO_2 Electrodes

This study, in which the capacity of the MnO_2^* electrode was collected within varying limits of discharge potentials, showed that modified materials can also be rendered non-rechargeable, if the specie(s) produced at the composition of approximately $MnO_{1.8}$ is allowed to accumulate. It has also been shown that the reduction mechanism of the MnO_2^* electrodes differs from the proton-hopping mechanism established for conventional MnO_2 electrodes. The latter proceeds in two clearly separate stages, i.e., the $Mn^{3+} \Rightarrow Mn^{2+}$ reduction does not begin before a substantial amount of Mn^{4+} had been converted to Mn^{3+}. For modified materials, the second electron reduction begins already when only a small fraction of Mn^{4+} was converted to Mn^{3+}. This may prevent the accumulation of the non-rechargeable Mn^{3+} specie(s) responsible for the irreversible behavior of the conventional MnO_2 electrodes.

3.5 Construction of Li-MnO_2^* Cells

The incorporation of the dehydrated MnO_2^* with lithium metal in nonaqueous solvents is very attractive from the point of having a rechargeable battery of high power density.

A collaborative research agreement was established with an outside laboratory that possesses the equipment needed to fabricate lithium cells. Twelve AA size cells having a spiral configuration were constructed with standard lithium negative technology and the MnO_2^* positive. The composition of the cathode mix consisted of 70 wt% MnO_2^*, 22 wt% carbon and 8 wt% Teflon. A large excess of lithium over MnO_2^* (7:1) was used. The cells were filled with 1.4 M $LiAsF_6$ electrolyte in 2-Methyl Tetrahydrofuran solvent. Two different kinds of separators were used in these cells. Six cells were constructed with Mead Glass fiber separator (designated "WN") and six with Rayperm 200/60 Tefzel (designated "SP"). These cells showed open circuit voltage (OCV) in the range of 3.1 to 3.4 V (Table 1). The performance of two cells, tested, was unsatisfactory, however. During the first discharge, a complete discharge of the capacity could not be obtained. This

indicated a condition equivalent to an internal shorting. The exact reason of this behavior could not be determined at this time.

REFERENCES

1. Y-F. Y. Yao, U.S. Patent No. 4,520,005 (1985).

2. Y-F. Y. Yao, N. Gupta and H.S. Wroblowa, J. Electroanal. Chem., 223 (1987) 107.

3. H.S. Wroblowa, N. Gupta, J. Electroanal. Chem., 238 (1987) 93.

4. R.G. Burns and V.M. Burns, in "Manganese Dioxide Symposium", Vol. 2 (Tokyo 1980), Paper No. 6, pp. 97-112.

5. P.C. Foller, J. Appl Electrochem., 17 (1987) 1296.

6. P. Stonehart, private communication, 1987.

TABLE 1

Cell #	Wt. Empty g	Wt. Full g	Wt. Electrolyte g	OCV(8/5/88) V	OCV(8/8/88) V	Separator Designation
1	11.720	15.449	3.729	3.11	3.15	WN
2	11.851	15.251	3.400	3.12	3.39	WN
3	11.856	15.325	3.496	3.40	3.39	WN
4	11.673	15.232	3.559	3.37	2.11	WN
5	12.128	15.666	3.538	3.40	3.38	WN
6	11.426	15.113	3.687	3.38	3.38	WN
7	10.459	13.981	3.522	3.13	3.23	SP
8	10.479	13.875	3.396	3.13	3.22	SP
9	10.296	14.480	4.184	3.14	3.17	SP
10	10.465	14.174	3.709	3.12	3.20	SP
11	10.644	14.190	3.546	3.12	3.17	SP
12	10.469	14.148	3.679	3.12	3.19	SP

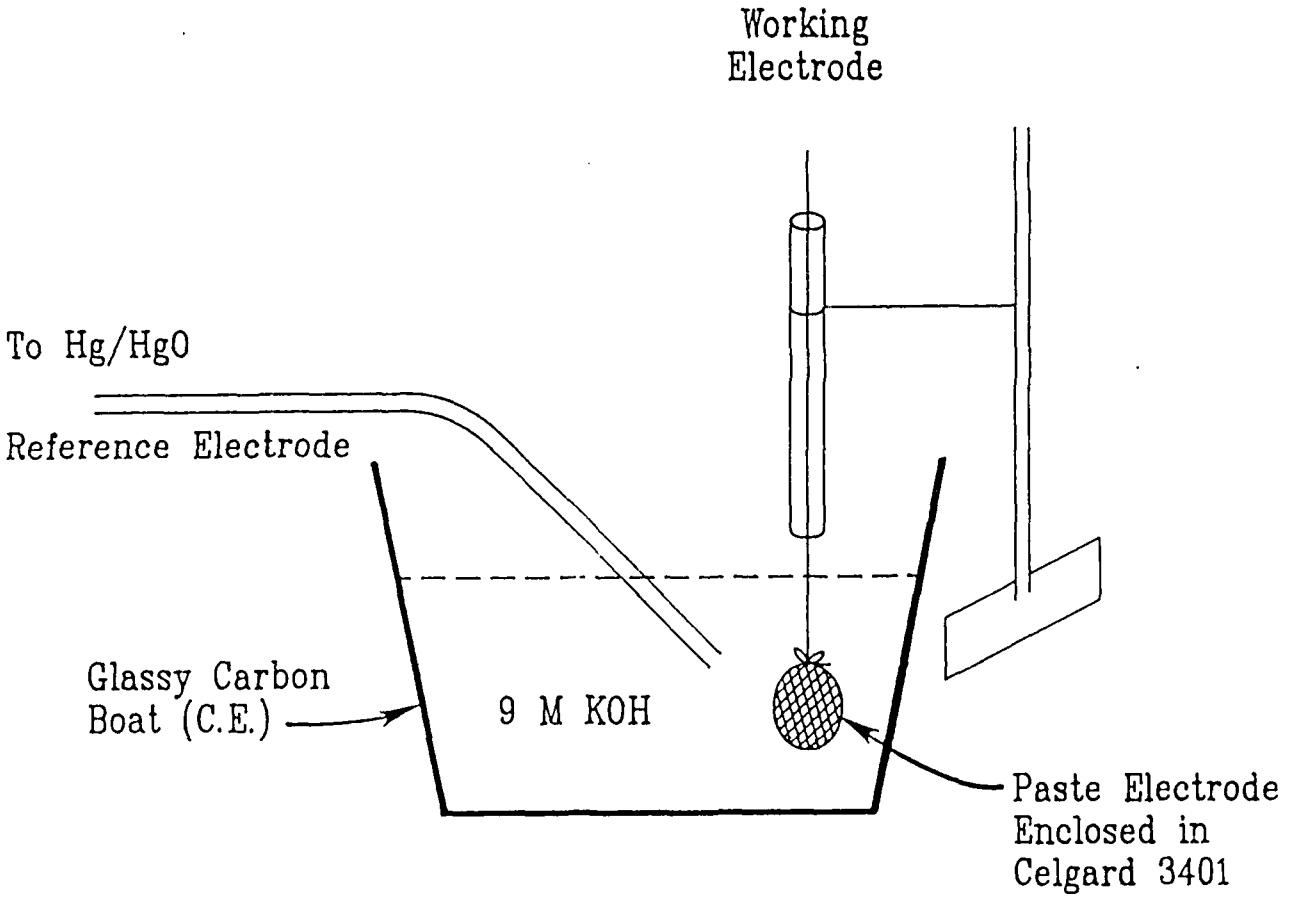

Figure 1. Sketch of the half-cell assembly with a "bundle" type MnO_2* electrode

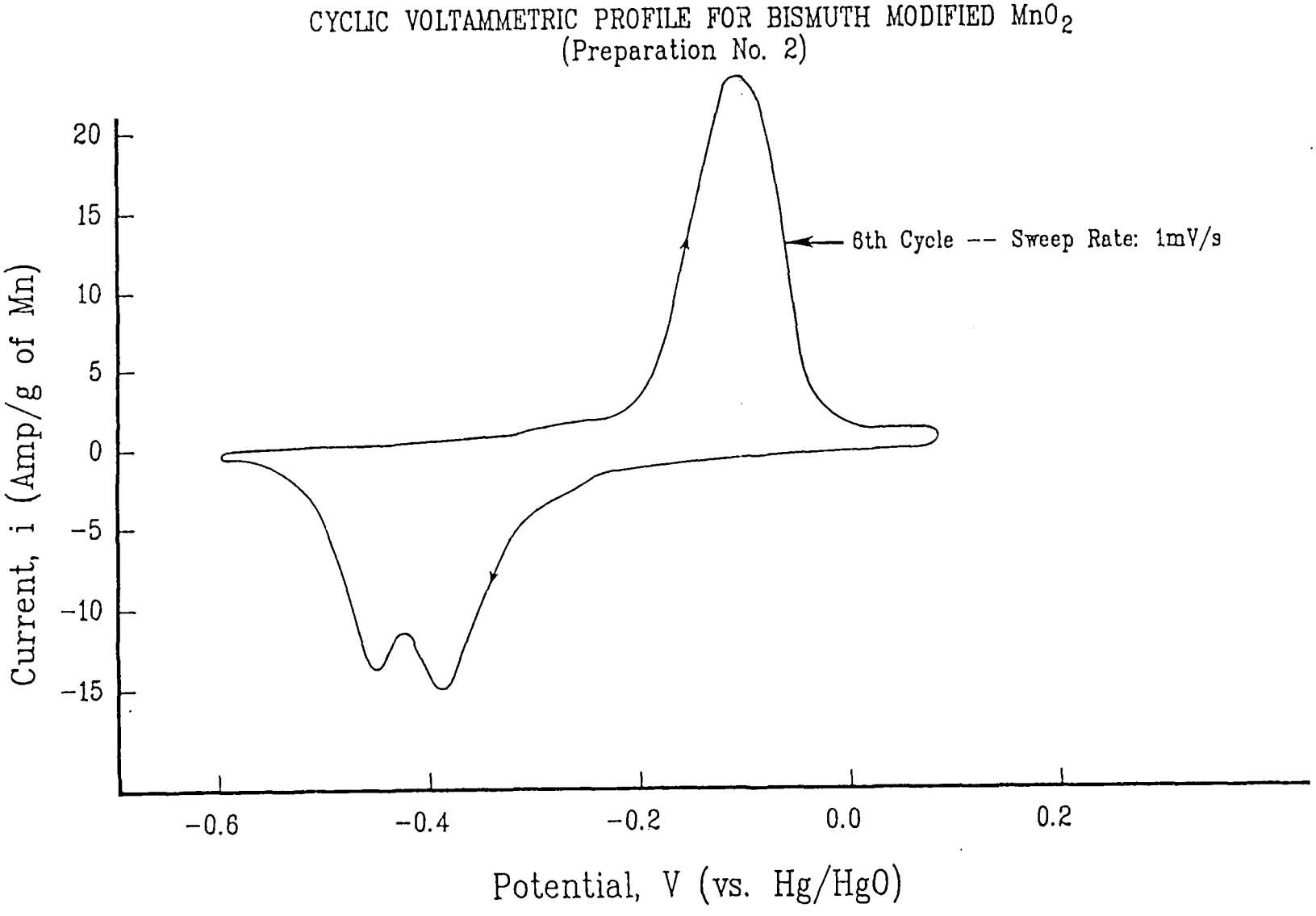

Figure 2. Potentiodynamic current-potential scan of the MnO_2* electrode

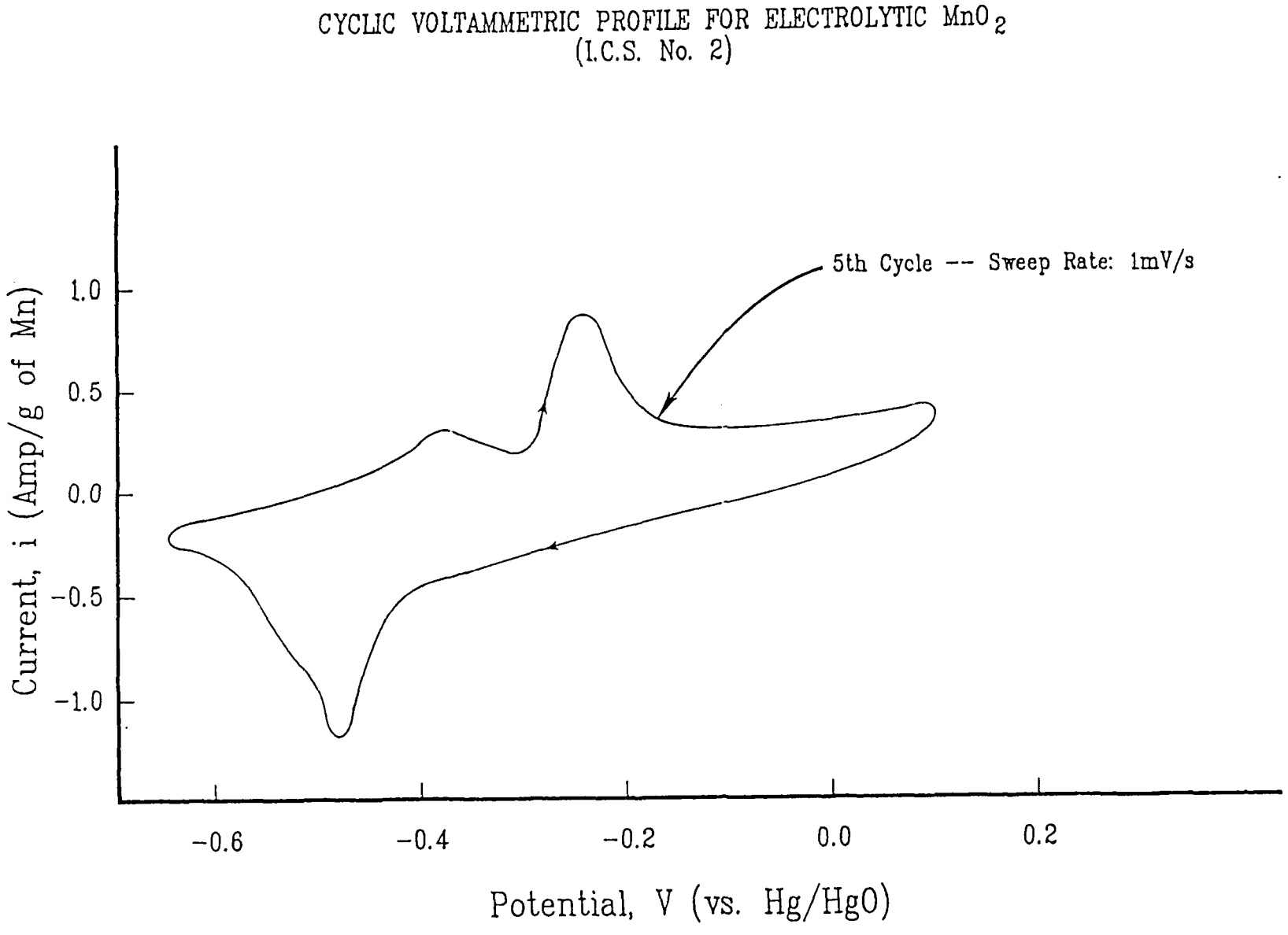

Figure 3. Potentiodynamic current-potential scan of electrolytic MnO_2 (I.C. No.2)

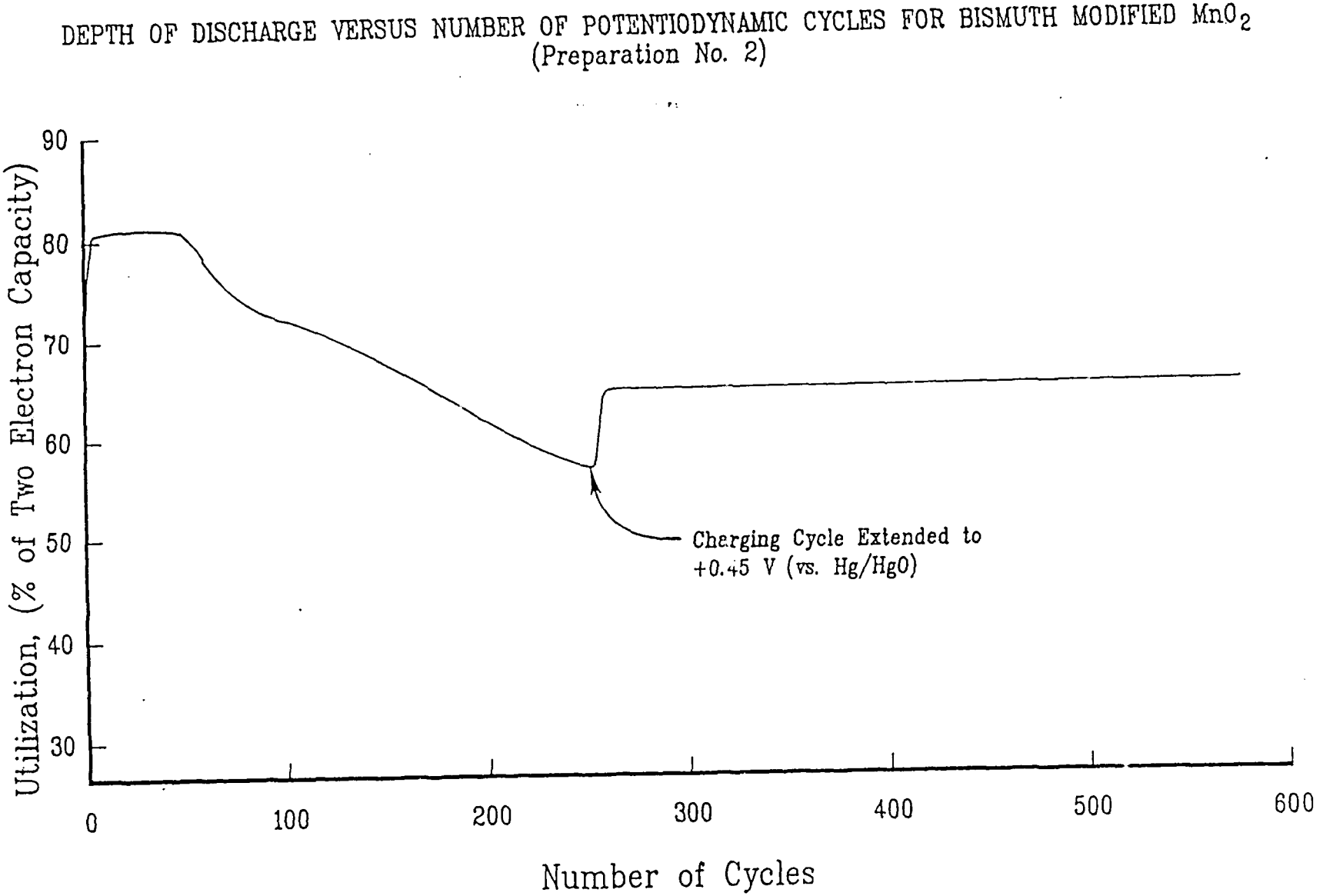

Figure 4. Fraction of the theoretical two electron capacity of the MnO_2* electrode as a function of cycle number during potentiodynamic cycling.

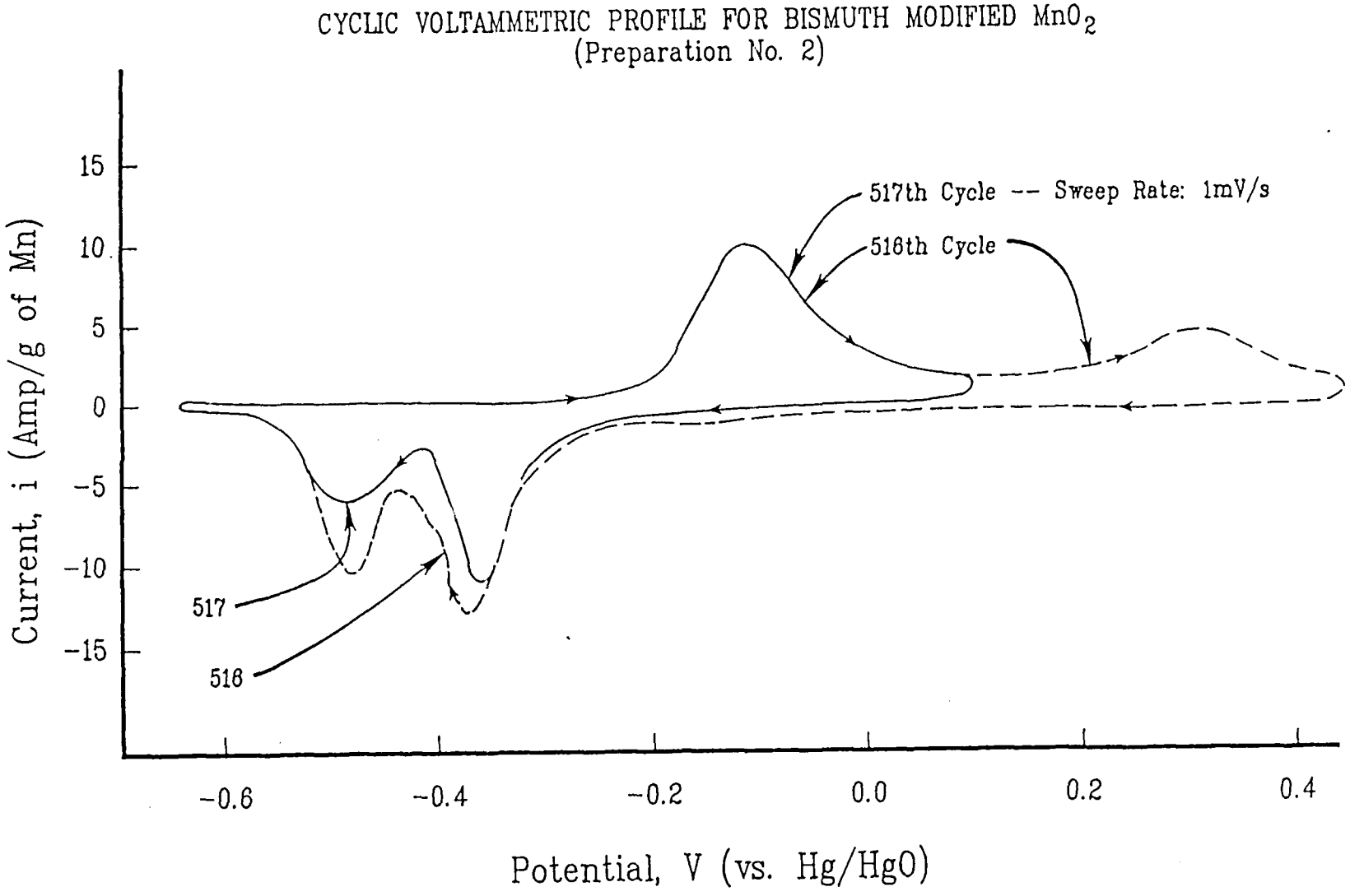

Figure 5. Potentiodynamic current-potential scans of the MnO_2^* electrode showing the splitting of anodic peaks. The shape of cathodic peaks remain the same.

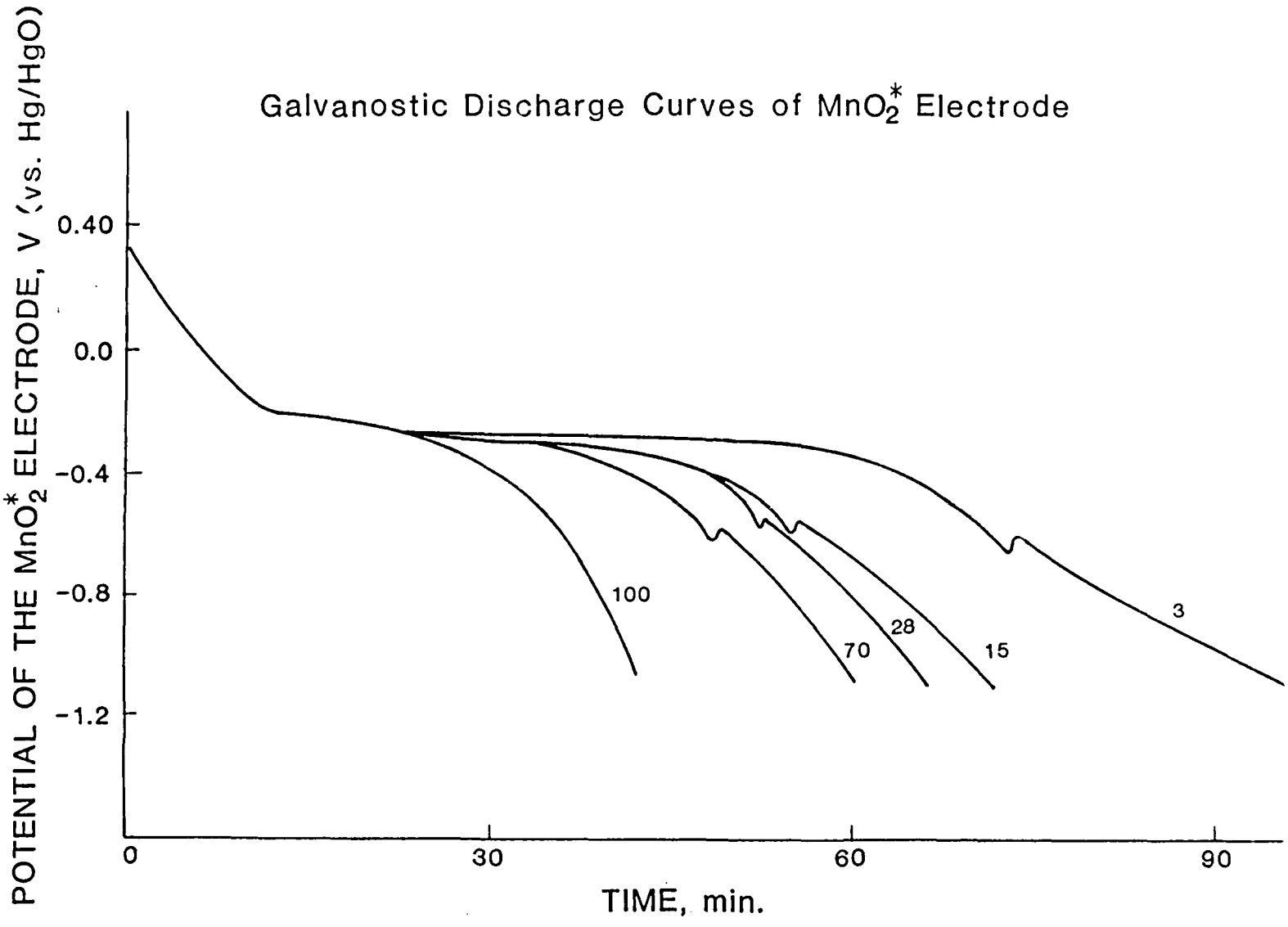

Figure 6. Constant current discharge curves of the MnO_2^* electrode in the flat cell. Cycle number shown on the curves. Electrtode mix was MnO_2: graphite: AcB in the proportion 1:9:1. Counter electrode: Ni/NiOOH. $^id = ^ic = 10$ mA of 653 mA/g of Mn. Polarization limits: +0.3 to -1.1 V.

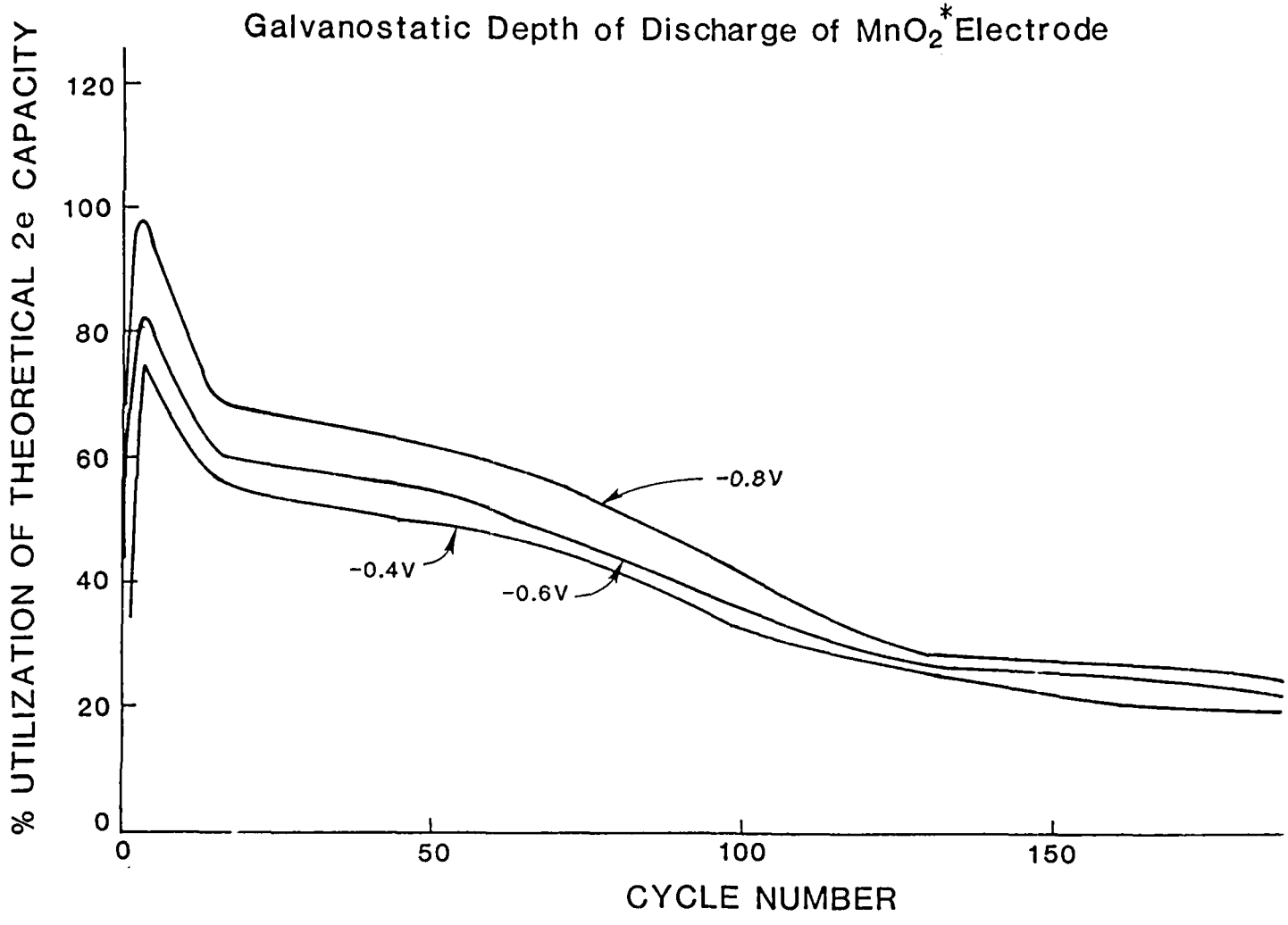

Figure 7. Utilization of the MnO_2^* electrode of Fig. 6 at various cut-off voltages as a function of cycle number during galvanostatic cycling in the flat cell.

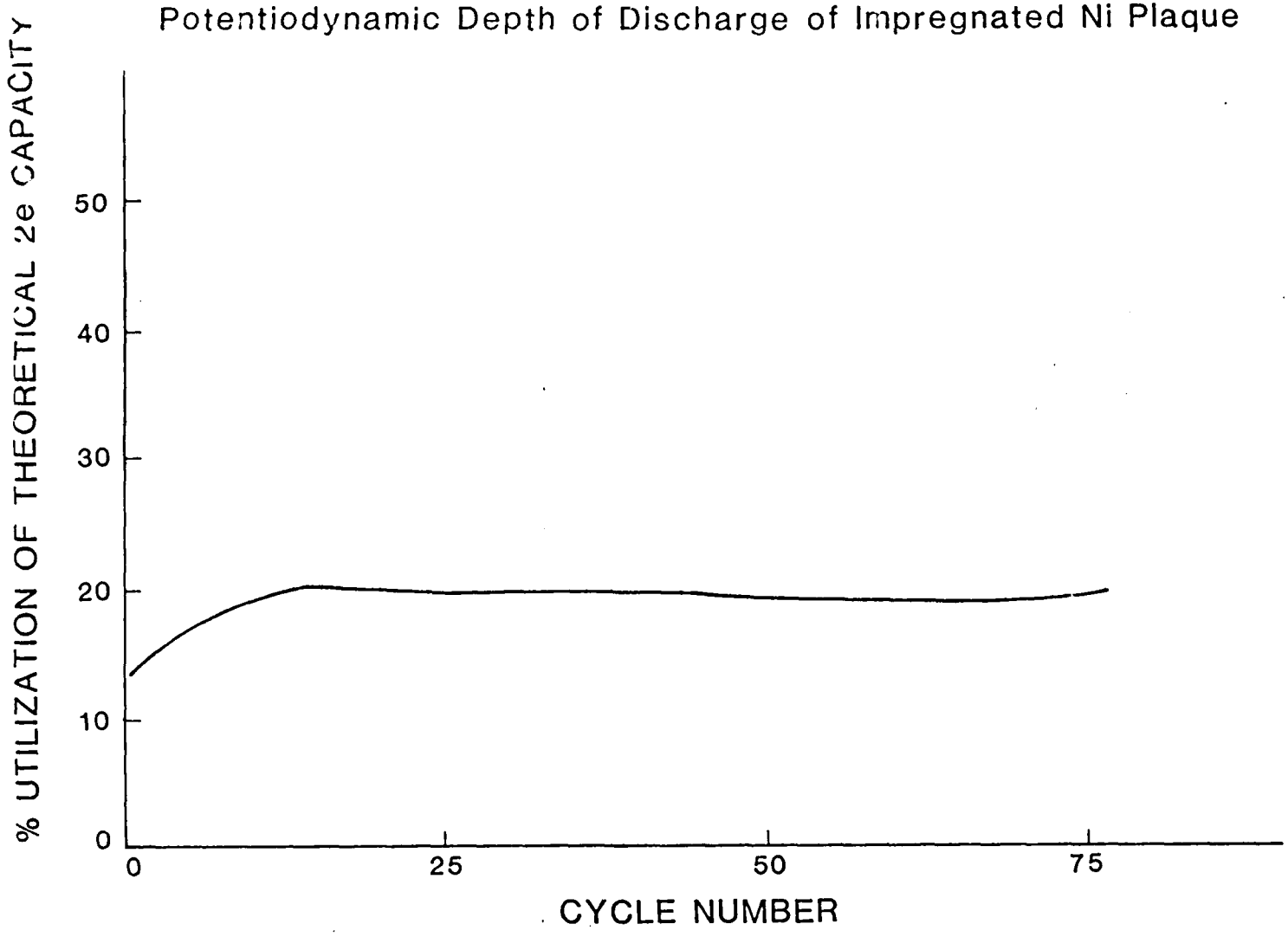

Figure 8. Utilization of the MnO_2^* impregnated Ni plaque as a function of cycle number during potentiodynamic cycling in the flat cell. Counter electrode: Ni/NiOOH. Amount of MnO_2^*: 164 mg.

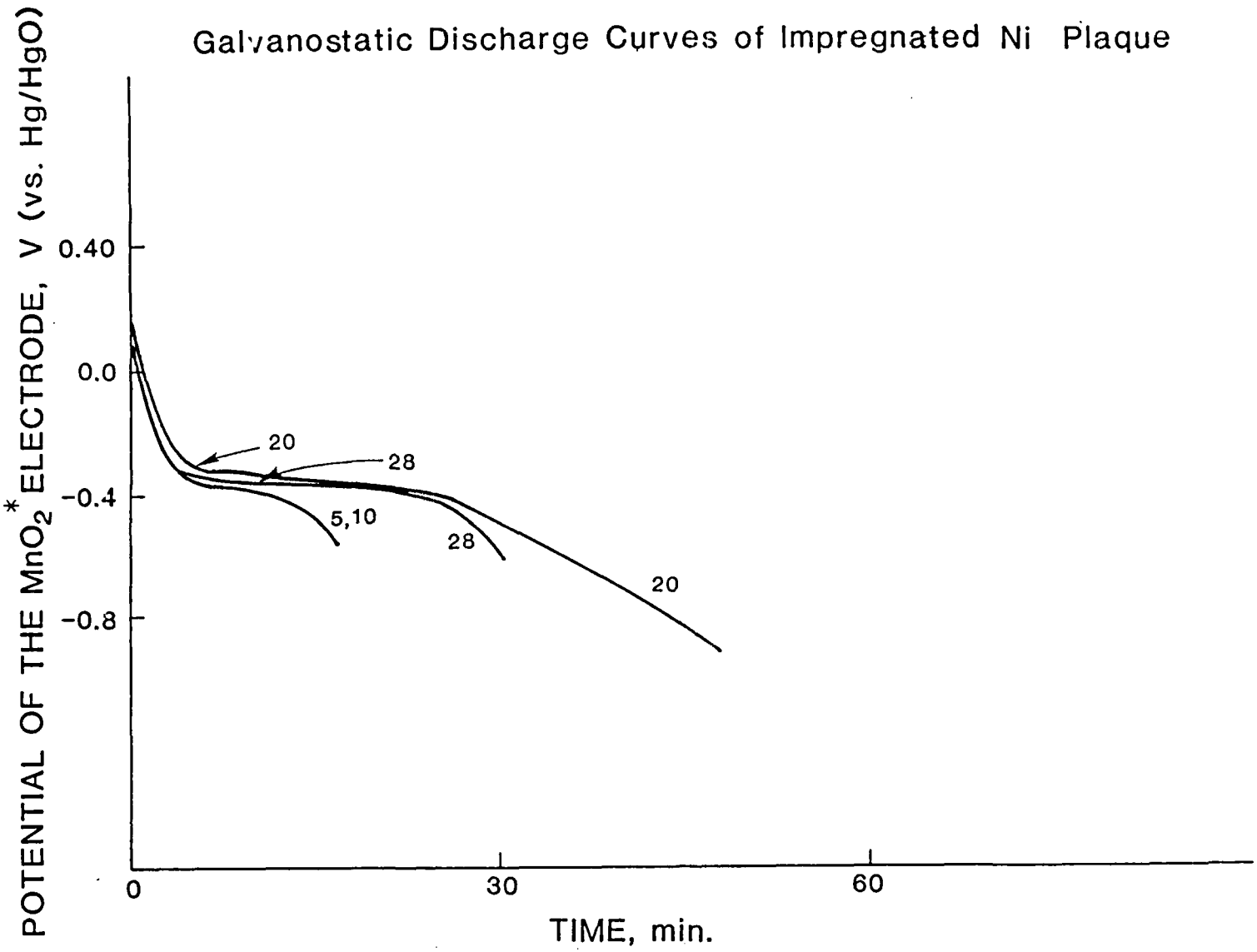

Figure 9. Constant current discharge curves of MnO_2* impregnated Ni plaque. Cycle numbers shown on the curves. $i_d = i_c$ = 50mA = 625 mA/g of Mn. Polarization limits: Cycles 1 to 13, +0.2 to -0.6V; Cycles 14 to 23, +0.2 to -0.9V; Cycles 24 to 28, +0.2 to -0.6V.

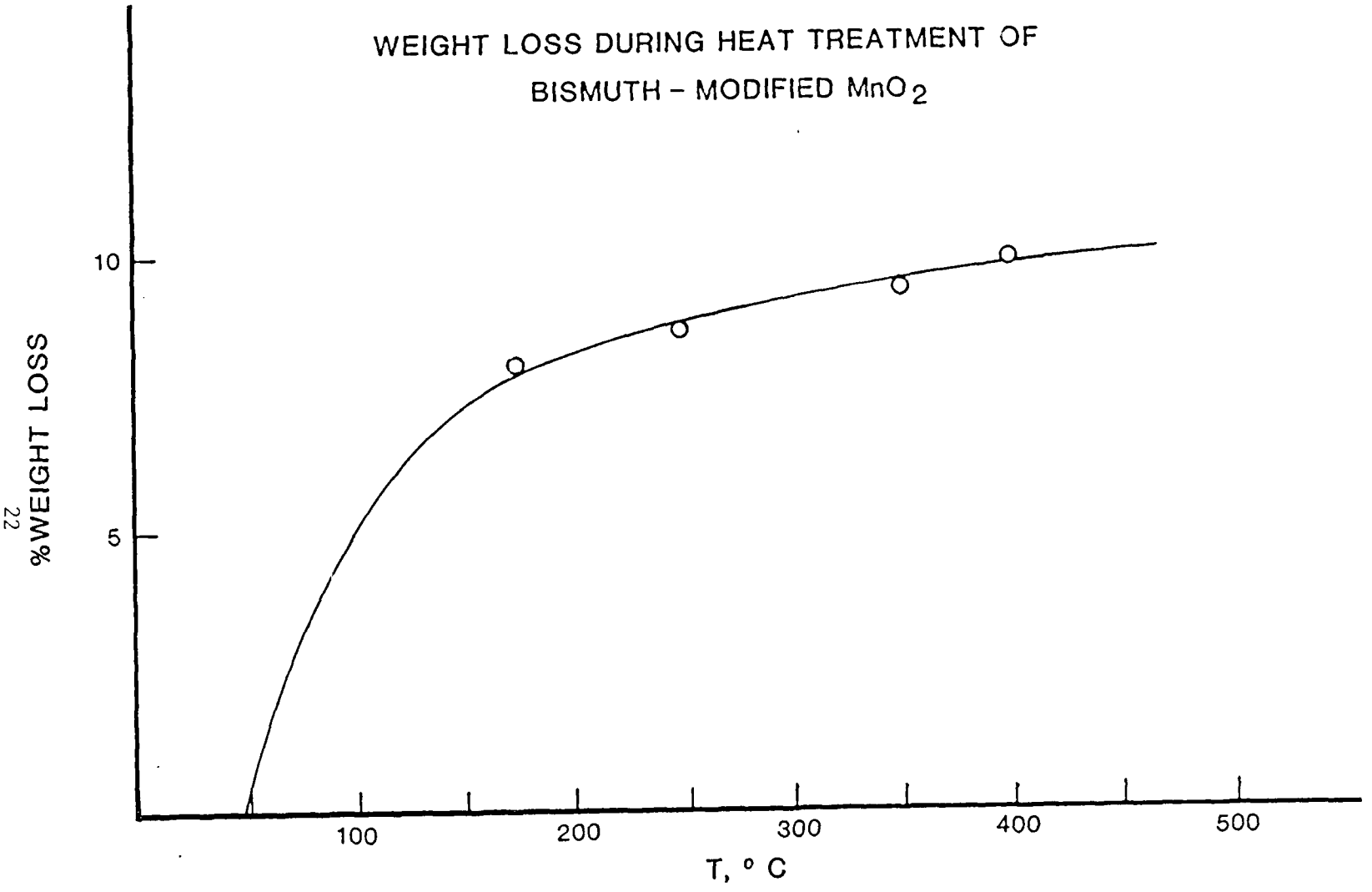

Figure 10. Weight loss behavior of the MnO_2* material during heat treatment.

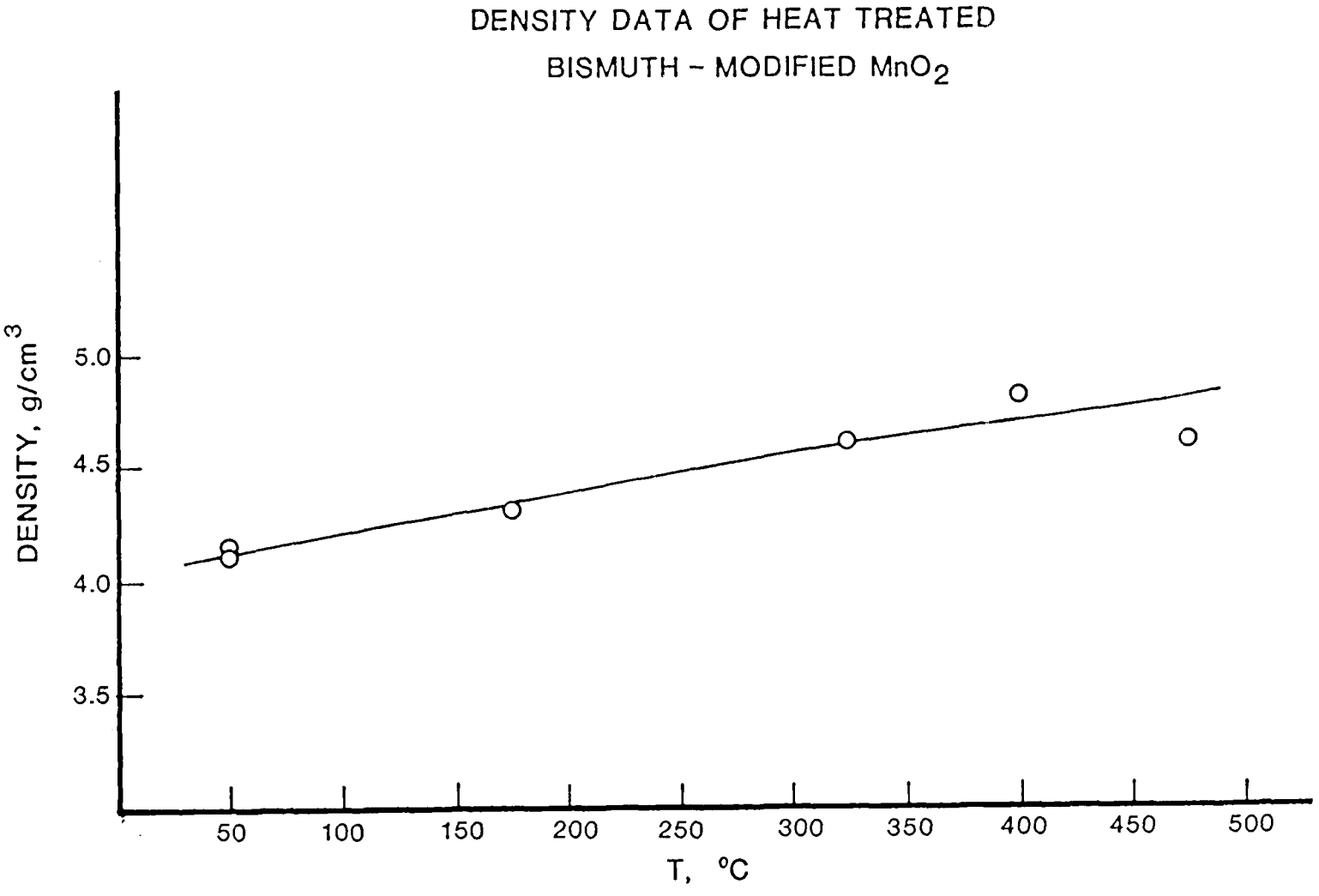

Figure 11. Density of the MnO_2* material as a function of heat treatment temperature.

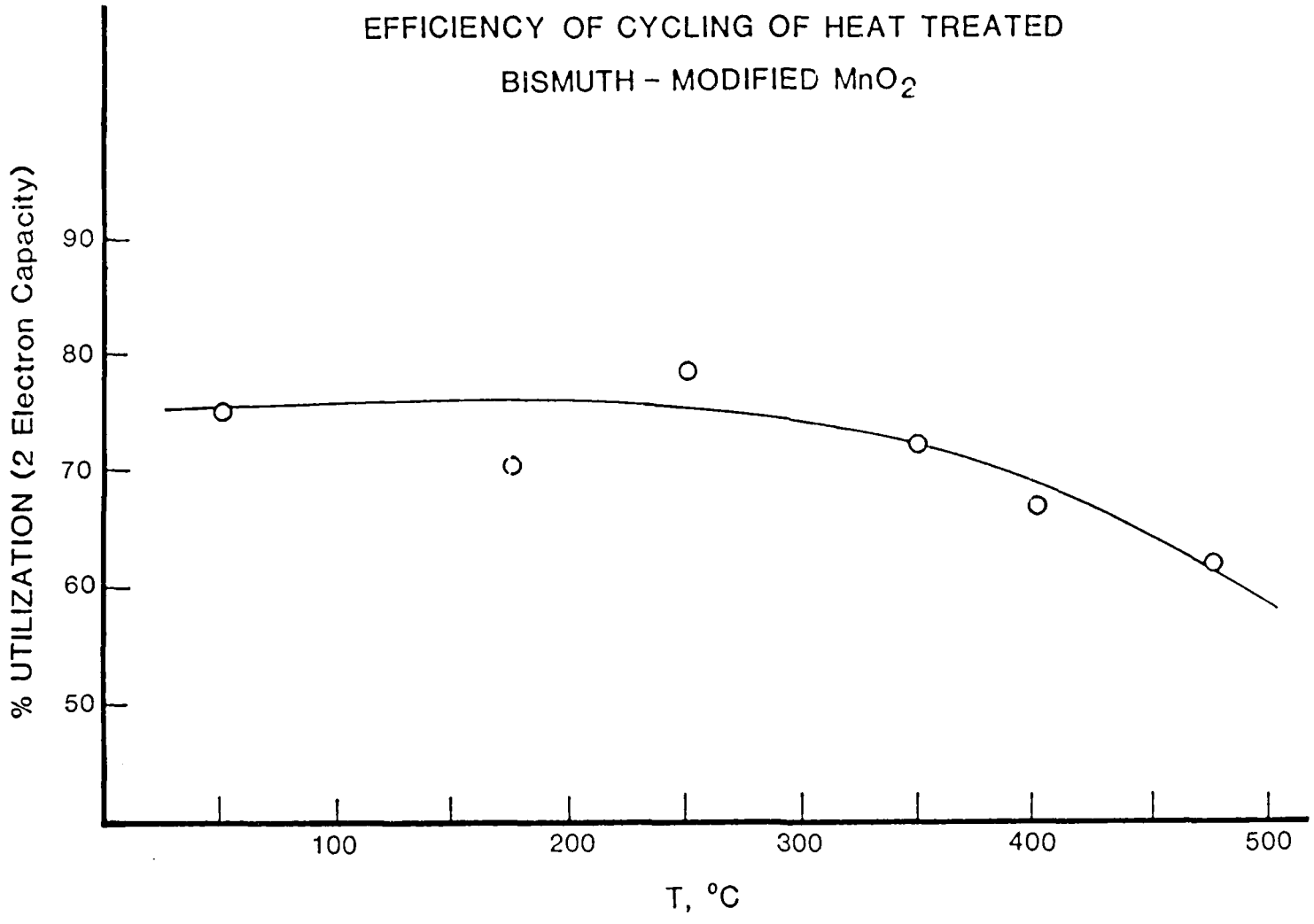

Figure 12. Change in utilization of the MnO_2* material as a function of heat treatment temperature.

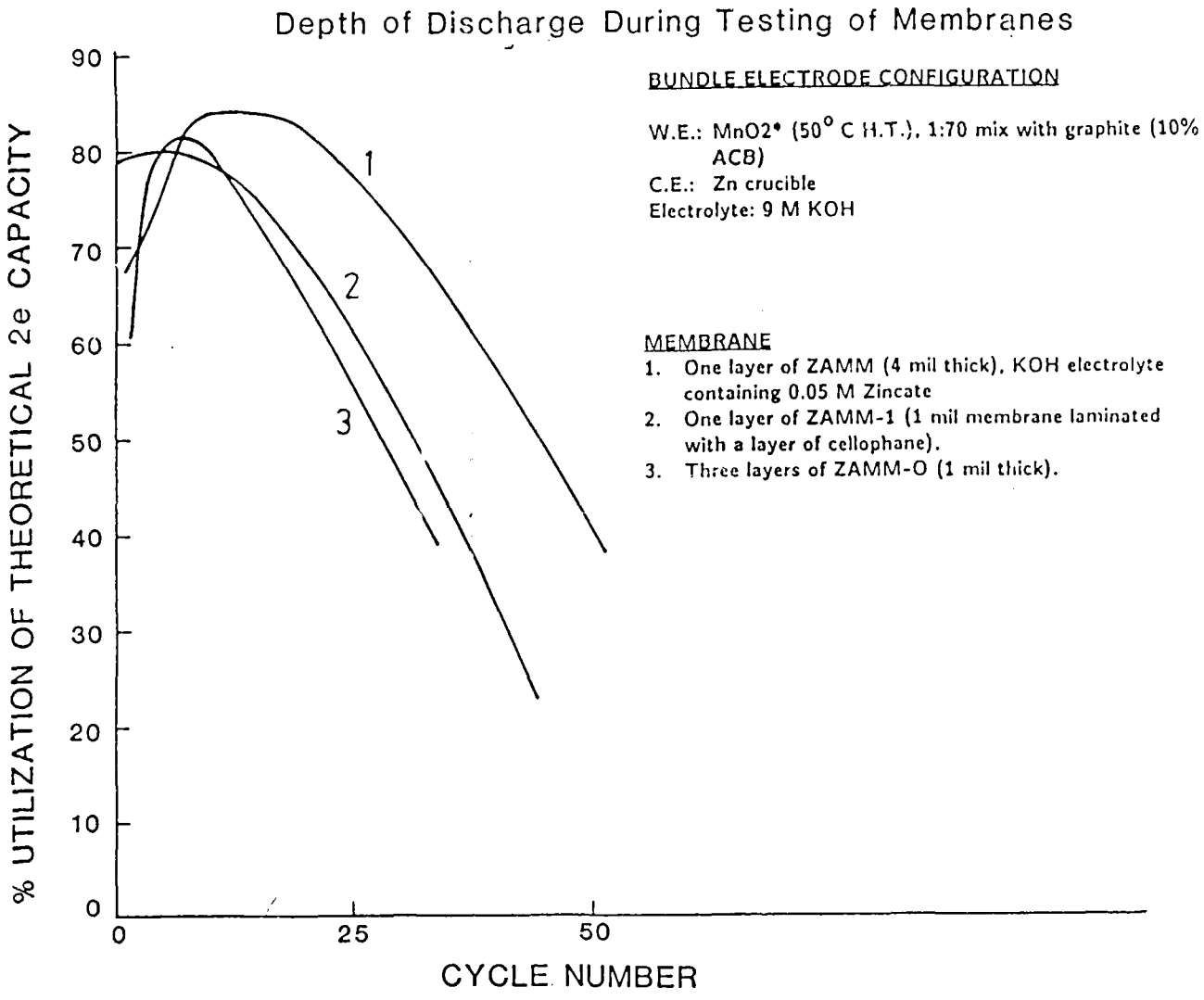

Figure 13. Utilization of the MnO_2^* electrode during potentiodynamic cycling in the bundle cell of Fig. 1. Effects of ZAMM membranes of different thicknesses are illustrated with Zn counter electrodes in the cells.

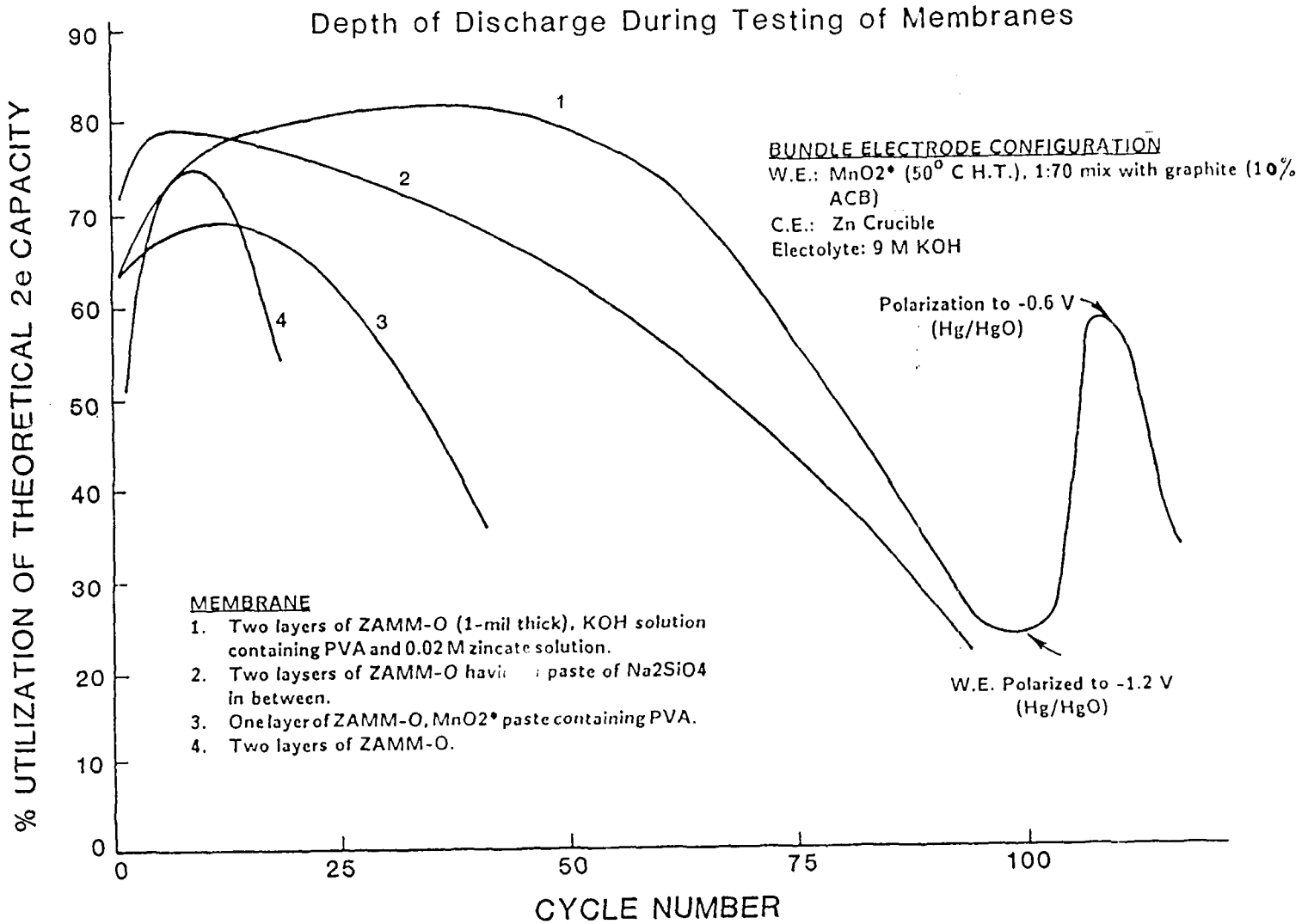

Figure 14. Utilization of the MnO_2^* electrode during potentiodynamic cycling in the bundle cell of Fig. 1. Effects of membrane, zincate anion and additives are illustrated with Zn counter electrodes in the cells. Membrane tested was ZAMM-O (1 mil thick).

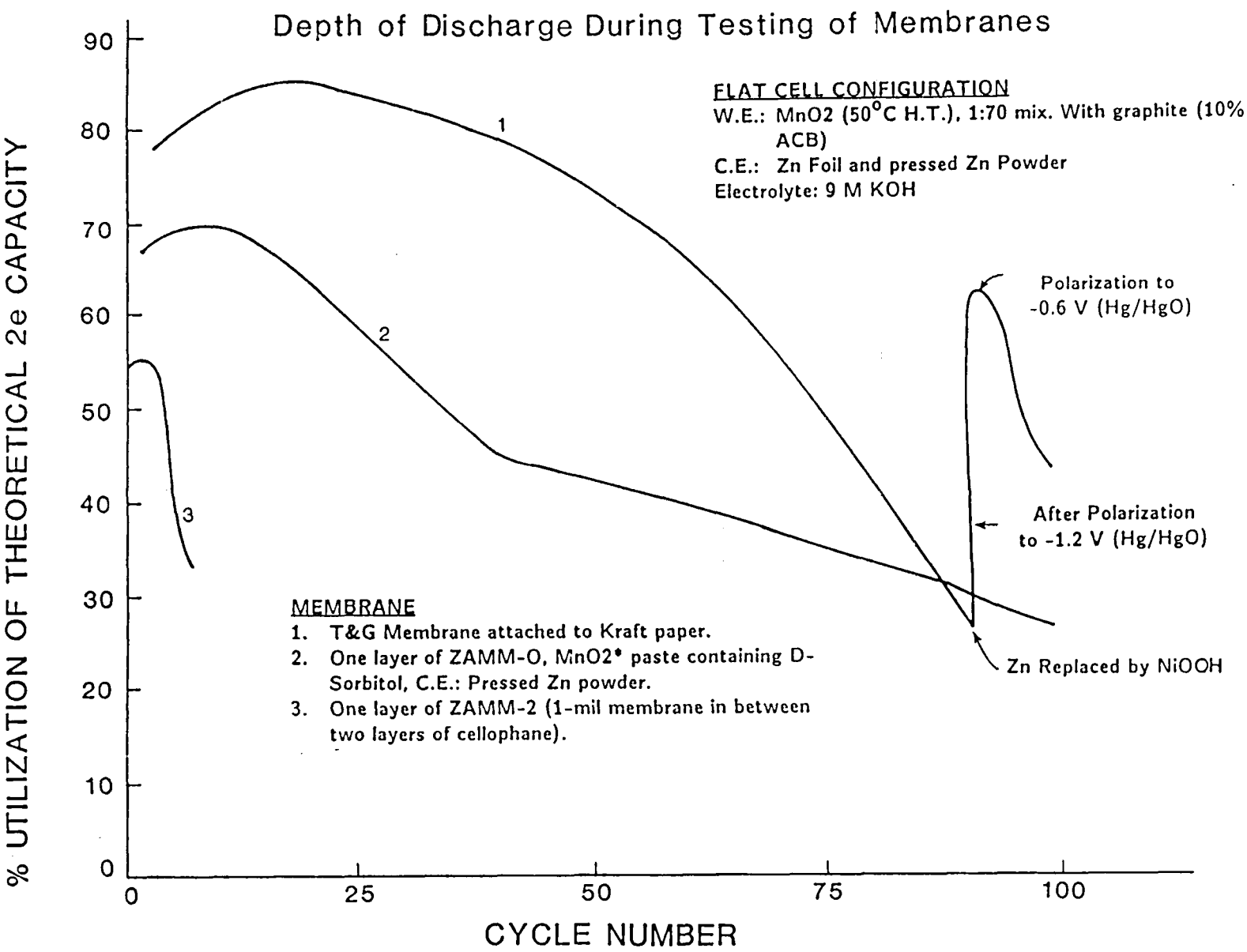

Figure 15. Utilization of the MnO_2* electrode during potentiodynamic cycling in the flat cell. Effects of ZAMM and T and G membranes are illustrated with Zn counter electrodes in the cells.

MATERIAL INSPECTION AND RECEIVING REPORT	1. PROC. INSTRUMENT IDEN (CONTRACT) (ORDER) NO.	6. INVOICE NO. DATE	7. PAGE 1 OF 1
	N00014-87-C-0662		8. ACCEPTANCE POINT D

2. SHIPMENT NO.	3. DATE SHIPPED	4. B/L TCN	5. DISCOUNT TERMS
EMT 0004Z	16Sept88		

9. PRIME CONTRACTOR CODE	10. ADMINISTERED BY CODE
0BAA8 Ementeck, Inc. Rt. 5, Box 946B College Station, TX 77840	S4404A DCASMA-San Antonio 615 East Houston Street P.O. Box 1040 San Antonio, TX 78294-1040

11. SHIPPED FROM (If other than 9) CODE / FOB:	12. PAYMENT WILL BE MADE BY CODE
See Block 9	S4403A DCASR - Dallas 1200 Main Street Dallas, TX 75202-4399

13. SHIPPED TO CODE	14. MARKED FOR CODE
Office of Naval Research Code 1113ES 800 North Quincy Street Arlington, VA 22217-5000 Attn: Dr. Robert Nowak	

15. ITEM NO.		16. STOCK/PART NO. DESCRIPTION (Indicate number of shipping containers-type of container-container number.)	17. QUANTITY SHIP'D/REC'D*	18. UNIT	19. UNIT PRICE	20. AMOUNT
0001	AD	Final Technical Report	01	ea	12,485.00	12,485.00
		Distribution to: Administrative Contracting Officer	01	ea		
		Director, Naval Research Laboratory Attn Code 2627	01	ea		
		Defense Technical Information Center	12	ea		

21. PROCUREMENT QUALITY ASSURANCE

A. ORIGIN — ☐ PQA ☐ ACCEPTANCE of listed items has been made by me or under my supervision and they conform to contract, except as noted herein or on supporting documents.

DATE | SIGNATURE OF AUTH GOVT REP

TYPED NAME AND OFFICE

B. DESTINATION — ☒ PQA ☒ ACCEPTANCE of listed items has been made by me or under my supervision and they conform to contract, except as noted herein or on supporting documents.

DATE | SIGNATURE OF AUTH GOVT REP

TYPED NAME AND TITLE

22. RECEIVER'S USE

Quantities shown in column 17 were received in apparent good condition except as noted.

DATE RECEIVED | SIGNATURE OF AUTH GOVT REP

TYPED NAME AND OFFICE

*If quantity received by the Government is the same as quantity shipped, indicate by (✓) mark, if different, enter actual quantity received below quantity shipped and encircle.

23. CONTRACTOR USE ONLY

Upon completion, please return original DD 250 to Block #9.

DD FORM 250

REPLACES EDITION OF 1 AUG 67 WHICH MAY BE USED